

DOI: 10.1002/cbic.200500452

# Structure–Activity Studies in a Family of $\beta$ -Hairpin Protein Epitope Mimetic Inhibitors of the p53–HDM2 Protein–Protein Interaction

Rudi Fasan,<sup>[a]</sup> Ricardo L. A. Dias,<sup>[a]</sup> Kerstin Moehle,<sup>[a]</sup> Oliver Zerbe,<sup>[a]</sup> Daniel Obrecht,<sup>[b]</sup> Peer R. E. Mittl,<sup>[c]</sup> Markus G. Grütter,<sup>[c]</sup> and John A. Robinson<sup>\*[a]</sup>

*Inhibitors of the interaction between the p53 tumor-suppressor protein and its natural human inhibitor HDM2 are attractive as potential anticancer agents. In earlier work we explored designing  $\beta$ -hairpin peptidomimetics of the  $\alpha$ -helical epitope on p53 that would bind tightly to the p53-binding site on HDM2. The  $\beta$ -hairpin is used as a scaffold to display energetically hot residues in an optimal array for interaction with HDM2. The initial lead  $\beta$ -hairpin mimetic, with a weak inhibitory activity ( $IC_{50} = 125 \mu M$ ), was optimized to afford cyclo-(L-Pro-Phe-Glu-6ClTrp-Leu-Asp-Trp-Glu-Phe-D-Pro) (where 6ClTrp = L-6-chlorotryptophan), which has*

*an affinity almost 1000 times higher ( $IC_{50} = 140 nM$ ). In this work, insights into the origins of this affinity maturation based on structure–activity studies and an X-ray crystal structure of the inhibitor/HDM2(residues 17–125) complex at 1.4 Å resolution are described. The crystal structure confirms the  $\beta$ -hairpin conformation of the bound ligand, and also reveals that a significant component of the affinity increase arises through new aromatic/aromatic stacking interactions between side chains around the hairpin and groups on the surface of HDM2.*

## Introduction

The disruption of protein–protein interactions by synthetic molecules currently represents one of the most challenging targets in chemical biology and medicinal chemistry. The relatively large surface areas and the dynamic natures of protein surfaces currently conspire to make inhibitor design very difficult. Mutagenesis studies repeatedly suggest, however, that the high affinities of many protein–protein interactions do not simply represent the sums of many weak interactions spread evenly across the interfaces. Rather, smaller subsets of energetically important residues—the so-called hot-spot residues—are typically found at protein interfaces; these appear to cluster into modules and are juxtaposed across the interfaces.<sup>[1–7]</sup> This suggests an approach to the design of protein–protein interaction inhibitors based on attempts to mimic these clusters of hot residues in smaller, synthetic, protein epitope mimetics (PEMs). Conceivably, a peptidomimetic of hot-spot residues on one surface might retain the ability of the parent protein to interact with its cognate binding partner, and so act as an inhibitor. One structural scaffold frequently used in nature to display groups for protein recognition is the  $\beta$ -hairpin. In this work we explore how synthetic  $\beta$ -hairpin PEMs can be used to display a cluster of hot-spot residues in an optimal geometry for binding to a protein surface.

We showed earlier that  $\beta$ -hairpin loop sequences excised from various natural proteins can be transplanted onto a D-Pro-L-Pro hairpin-inducing template.<sup>[8–14]</sup> The resulting cyclic peptidomimetics are readily accessible by synthesis, and have been shown to adopt  $\beta$ -hairpin conformations very similar to


those found in the natural protein. We have also reported how a  $\beta$ -hairpin PEM can be used as a mimetic of an  $\alpha$ -helical epitope, and thus be used to generate inhibitors of the p53–HDM2 interaction.<sup>[15]</sup> Inhibitors of the interaction between the p53 tumor suppressor protein and its natural human inhibitor HDM2 are attractive as potential anticancer agents.<sup>[16]</sup> Hot residues aligned along one face of the helical p53 peptide (Phe19, Trp23, and Leu26) fill hydrophobic pockets on the surface of HDM2 (Figure 1).<sup>[17]</sup> In the design of an inhibitor, these key residues were incorporated at appropriate positions along one strand of a  $\beta$ -hairpin. The first  $\beta$ -hairpin mimetic **1** (Figure 1) designed in this way showed only weak inhibitory activity

[a] Dr. R. Fasan,<sup>+</sup> Dr. R. L. A. Dias,<sup>+</sup> Dr. K. Moehle, Dr. O. Zerbe, Prof. J. A. Robinson  
Institute of Organic Chemistry, University of Zürich  
Winterthurerstrasse 190, 8057 Zürich (Switzerland)  
Fax: (+41) 1635-6833  
E-mail: robinson@oci.unizh.ch

[b] Dr. D. Obrecht  
Polyphor AG,  
4123 Allschwil (Switzerland)

[c] Dr. P. R. E. Mittl, Prof. M. G. Grütter  
Biochemistry Institute, University of Zürich  
Winterthurerstrasse 190, 8057 Zürich (Switzerland)

[\*] These authors contributed equally to this work.

 Supporting information for this article is available on the WWW under <http://www.chembiochem.org> or from the author: results of chemical-shift mapping experiments, NMR assignments, ROEs of mimetics **1** and **63**, and experimental analytical data.

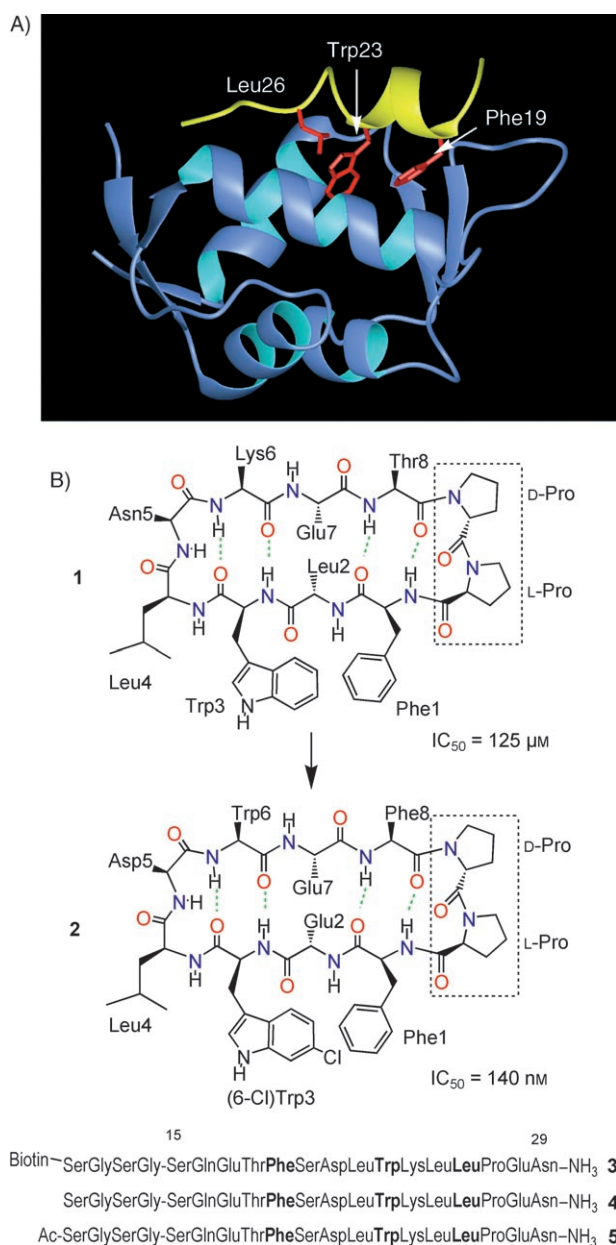


**Figure 1.** A) Ribbon representation of the p53-HDM2 complex (orange/blue; PDB file 1YCR), showing the p53 side chains of Phe19, Trp23, and Leu26 (red). B) Structures of lead mimetics and p53-derived peptides. The inhibitory activities ( $IC_{50}$ ,  $\mu\text{M}$ ) of the mimetics are also shown.

( $IC_{50} = 125 \mu\text{M}$ ). However, it was possible to find improved variants, including the mimetic **2**<sup>[18]</sup> showing an affinity almost 1000 times higher ( $IC_{50} = 140 \text{ nM}$ ).<sup>[15]</sup> In this work, insights into the origins of this affinity maturation—based on structure-activity studies and an X-ray crystal structure of the **2**/HDM2 (residues 17–125) complex at 1.4 Å resolution—have been obtained. The **2**/HDM2 crystal structure confirms the  $\beta$ -hairpin conformation of the bound ligand, and the successful mimicry of the Phe/Trp/Leu hotspot residues in bound p53 by **2**. A significant component of the affinity increase from **1** to **2**, however, is seen to arise through new aromatic-aromatic stacking interactions, not seen in the p53/HDM2 complex, that side

chains around the hairpin in **2** make with groups on the surface of HDM2. This mechanism of binding is of interest, since it might conceivably be exploitable in the design of other PEM molecules targeting other protein surfaces.

## Results

### 1. Binding assays

All mimetics were assayed for p53/HDM2 inhibitory activity by a solution-phase competition assay with a surface plasmon resonance biosensor (BIAcore). The biotinylated peptide **3**, containing residues 15–29 from p53, with a SerGlySerGly linker, was immobilized on a streptavidin-coated biosensor chip. The partner used for assays comprised residues 17–125 of HDM2 with an N-terminal extension derived from the expression vector pET14b (Novagen) including a hexa-His tag and a thrombin cleavage site. This protein binds to the p53-peptide-sensor surface with a  $K_D$  value of 670 nM, determined by steady state analysis. For comparison, a  $K_D$  value of 600 nM was reported for the same interaction by titration calorimetry<sup>[17,19]</sup> and similar values were obtained by stopped-flow fluorimetry<sup>[19]</sup> ( $K_D = 580 \text{ nM}$ ) and fluorescence anisotropy ( $K_D = 700 \text{ nM}$ ).<sup>[20]</sup> These data indicate that the HDM2/p53-peptide interaction in this BIAcore assay is native-like and it is not affected significantly either by the His<sub>6</sub>-tag or by the BIAcore capturing method.

In competition binding assays, this HDM2 protein (250 nM) and increasing concentrations of the mimetic were injected over the p53-peptide-coated surface. Inhibition of protein binding to the surface causes a decrease in biosensor response. In this way, the  $IC_{50}$  values for the mimetic **1** and for the p53-derived peptide **4** were determined to be 125  $\mu\text{M}$  and 1.1  $\mu\text{M}$ , respectively.

### 2. Solution conformation of mimetic 1 and its interaction with HDM2

The design of mimetic **1** assumes that the molecule will adopt a regular  $\beta$ -hairpin conformation. The average solution structure of **1** in water was therefore investigated by NMR spectroscopy. The 1D <sup>1</sup>H NMR spectrum of **1** showed a single average conformer on the NMR timescale, with all peptide bonds *trans*. However, several key indicators suggested that the peptide was not adopting a regular 2:2  $\beta$ -hairpin conformation.<sup>[21]</sup> For example, several <sup>3</sup>J<sub>HN,H $\alpha$</sub>  coupling constants are < 7 Hz, rather than > 8.5 Hz as would be expected for residues in a regular  $\beta$ -structure. Also, no clear evidence for a stable  $\beta$ -turn at residues Leu4/Asn5 was seen, as would be expected at the tip of a regular  $\beta$ -hairpin; the Asn5–Lys6 *d*NN (*i*, *i*+1) ROE-derived distance restraint (3.9 Å) was larger than expected for a  $\beta$ -turn (< 3.0 Å). The detection of a cross-strand Glu2 H( $\alpha$ )-Glu7 H( $\alpha$ ) ROE, which would have been strong evidence for a  $\beta$ -hairpin structure, was not possible, due to partial overlap of these resonances, although several long-range ROEs were seen between side chains that are not adjacent in the sequence. The absence of a regular 2:2 hairpin conformation in **1** was also

supported by structure calculations performed with use of the available ROE and dihedral angle restraints. Low-energy DYANA conformers with distorted hairpin structures were obtained, and a hydrophobic cluster formed on one face of the molecule through stacking of the Phe1, Trp3, and Leu4 side chains (Figure 2 and Table 1). A hydrogen bond between NH of Phe1 and CO of Thr8 is present in some structures, as would be expected from the tight type II'  $\beta$ -turn adopted by the D-Pro-L-Pro template, but no regular 2:2  $\beta$ -hairpin conformation was found.

In order to confirm that **1** will interact with the expected p53-binding site on HDM2, chemical shift mapping was performed by  $^{15}\text{N},^1\text{H}$  heteronuclear single quantum correlation (HSQC) NMR spectroscopy.<sup>[22–24]</sup> This work was aided by the availability of published NMR assignments of HDM2.<sup>[25]</sup> HSQC spectra of  $^{15}\text{N}$ -labeled HDM2 were measured alone and in the presence of either **1** or the p53(15–29) peptide **5**. Upon addition of **5** a large number of HDM2  $^{15}\text{N},^1\text{H}$  cross-peaks were perturbed for residues located on the second half of the  $\alpha$ 2-helix (Tyr56–Thr63), the  $\beta$ 1'-strand (Gln71, Gln72, Val75), and the  $\beta$ 2'-strand (Phe91–Lys94) of HDM2. These residues define the Phe19, Trp23, and Leu26 sub-pockets of the p53-binding site

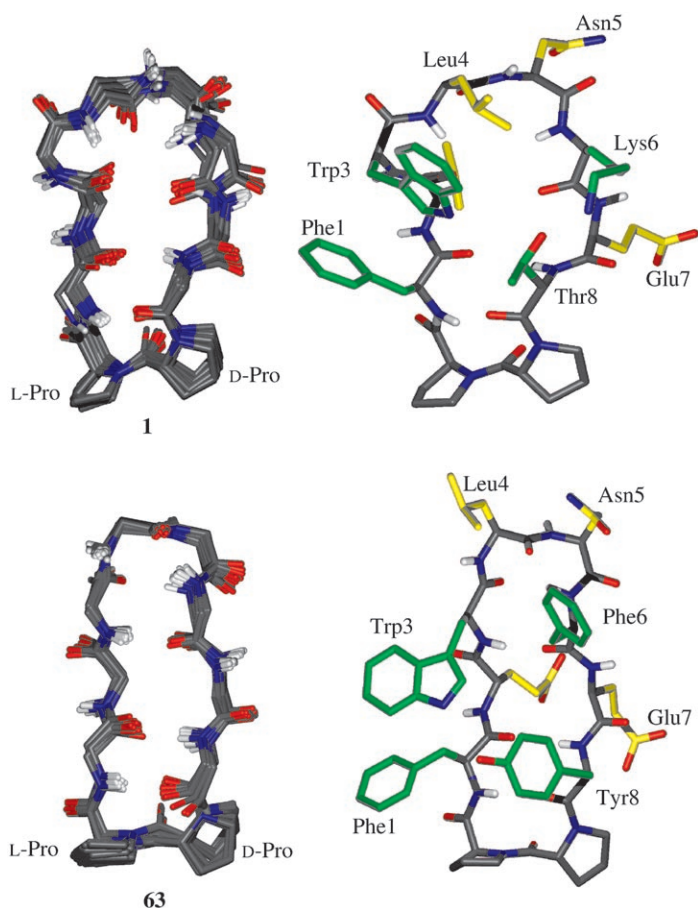


**Figure 2.** Superimposition of backbone atoms in the 20 low-energy DYANA solution NMR structures (Table 1) and one typical average NMR structure of mimetic **1** and mimetic **63**. A hydrophobic cluster is formed on one face of **1** through stacking of the Phe1, Trp3, and Leu4 side chains. A regular 2:2  $\beta$ -hairpin conformation is found in **63**.

**Table 1.** Summary of restraints used and statistics for the NMR structure calculations performed on mimetics **1** and **63** with DYANA.<sup>[77]</sup> The final 20 NMR structures are shown in Figure 2, and a list of the ROE restraints used is given in the Supporting Information.

Mimetic	<b>1</b>	<b>63</b>
ROE upper distance limits	95	116
intraresidue	27	31
sequential	40	39
medium- and long-range	28	46
dihedral angle restraints (HN,H $\alpha$ )	7	8
residual target function value [ $\text{\AA}^2$ ]	$1.00 \pm 0.06$	$0.58 \pm 0.05$
Mean rmsd values [ $\text{\AA}$ ]		
all backbone atoms	$0.44 \pm 0.18$	$0.32 \pm 0.17$
all heavy atoms	$1.08 \pm 0.22$	$1.06 \pm 0.22$
Residual ROE violation		
violation $> 0.22 \text{ \AA}$	11	0
maximum violation [ $\text{\AA}$ ]	0.25	–

in HDM2. Significant perturbations are also experienced by a set of residues further removed from the binding cleft: for example Leu34, Leu38, Val41 ( $\alpha$ 1-helix) and Leu27, Val28, Tyr48, Leu107, Val108 (central part of the  $\beta$ -strand at the end of the HDM2 cleft). Similar observations were reported recently by Fersht and co-workers.<sup>[26]</sup> In the presence of mimetic **1**, a smaller number of HDM2 amide resonances are perturbed, but these again lie mostly in and around the p53 binding cleft (see Supporting Information), including in the second half of the  $\alpha$ 2-helix. These data confirm that the mimetic **1** interacts with the p53-binding pocket on HDM2, although no information about the orientation of the bound ligand in the binding pocket could be obtained from this experiment.

### 3. Ligand optimization

The weak inhibitory activity of **1** might be due to the absence of a stable  $\beta$ -hairpin conformation in the free peptide, so attempts were made to stabilize a  $\beta$ -hairpin structure without altering the hot residues (Phe1, Trp3, and Leu4), which had earlier been shown by alanine scanning to be energetically important residues for binding of **1** to HDM2.<sup>[15]</sup> The first series of analogues made—mimetics **6–24** (Table 2)—contained various  $\beta$ -branched residues, glycine at the hairpin tip, and proline at position 7. In addition, a constrained analogue (**24**) was prepared, with two cysteines at positions 2 and 7 linked through an intramolecular disulfide bridge. The p53–HDM2 inhibitory activities revealed improvements of up to fivefold (mimetic **10**) relative to **1**. In general, an increase in the hydrophobic character of residue 8 was associated with an improved inhibitory activity. Mimetic **10** incorporates a Pro in position 7, although this replacement appeared to be rather disruptive in most cases, unless Ile was also present at position 8.

It was not possible to calculate NMR structures for all the mimetics, but  $^3J_{\text{HN,H}\alpha}$  coupling constants were measured from 1D  $^1\text{H}$  NMR spectra, in attempts to correlate  $^3J$  values typical of  $\beta$ -structure ( $> 8.5 \text{ Hz}$ ) with improved inhibitory activity. Unfortunately, no clear correlation was found. Indeed, for the most active peptide (mimetic **10**), broad NH peaks were ob-

**Table 2.** Library of p53 mimetics. Residues 1 to 8 are attached to a D-Pro-L-Pro template (see Figure 1B). Mean inhibitory activities (IC<sub>50</sub>, μM) and standard deviations derive from at least three independent SPR-based inhibition assay experiments.<sup>[a]</sup>

Mimetic	1	2	3	4	5	6	7	8	IC <sub>50</sub> [μM]
1	F	L	W	L	N	K	E	T	125 ± 8
6	F	L	W	L	N	K	E	I	104 ± 8
7	F	I	W	L	N	K	E	T	175 ± 14
8	F	I	W	L	N	K	E	I	47 ± 9
9	F	I	W	L	N	K	P	T	> 500
10	F	I	W	L	N	K	P	I	26 ± 3
11	F	I	W	L	K	K	P	I	88 ± 7
12	F	L	W	L	G	K	E	T	62 ± 5
13	F	L	W	L	G	K	E	I	50 ± 4
14	F	I	W	L	G	K	E	T	240 ± 19
15	F	I	W	L	G	K	E	I	69 ± 6
16	F	I	W	L	G	K	P	T	> 300
17	F	I	W	L	G	K	P	I	100 ± 8
18	F	L	W	L	N	G	E	T	127 ± 10
19	F	L	W	L	K	G	E	I	49 ± 1
20	F	I	W	L	K	G	E	T	138 ± 9
21	F	I	W	L	K	G	E	I	112 ± 7
22	F	I	W	L	K	G	P	T	400 ± 18
23	F	I	W	L	K	G	P	I	(~75) <sup>[b]</sup>
24	F	C	W	L	N	K	C	T	(≥200) <sup>[b]</sup>
25	F	L	W	L	N	Y	E	T	53 ± 2
26	F	K	W	L	N	Y	E	T	105 ± 8
27	F	E	W	L	N	Y	K	T	51 ± 4
28	F	K	W	L	N	Y	E	F	9.5 ± 2.4
29	F	K	W	L	N	Y	E	Y	12 ± 1
30	F	K	W	L	N	Y	E	Bip	37 ± 3
31	F	K	W	L	N	F	E	T	24 ± 2
32	F	K	W	L	N	Bip	E	T	63 ± 5
33	F	L	W	G	N	Y	E	T	59 ± 6
34	F	L	W	N	G	Y	E	T	175 ± 14
35	F	L	W	N	P	Y	E	T	140 ± 11
36	F	L	W	P	N	Y	E	T	63 ± 5
37	F	L	W	V	N	Y	E	T	68 ± 5
38	F	K	W	N	G	Y	E	F	27 ± 2
39	F	K	Bip	N	G	Y	E	T	40 ± 3
40	Bip	K	W	N	G	Y	E	T	33 ± 5
41	W	K	F	N	G	Y	E	T	350 ± 15
42	F	L	W	L	G	K	P	I	65 ± 1.9
43	F	L	W	L	N	Y	P	I	40 ± 7
44	F	L	W	L	N	F	P	I	175 ± 35
45	F	L	W	L	G	F	P	I	> 500
46	F	L	W	L	N	K	P	I	77 ± 3
47	F	E	W	L	G	K	P	I	64 ± 1
48	F	E	W	L	N	W	P	I	34 ± 4
49	F	E	W	L	N	F	P	I	36 ± 4
50	F	E	W	L	G	F	P	I	20 ± 5
51	F	E	W	L	N	Y	K	F	9.3 ± 0.4
52	F	E	W	L	N	F	K	Y	11.4 ± 0.1
53	F	E	W	L	N	F	K	W	26 ± 1
54	F	E	W	L	G	F	K	Y	18.2 ± 0.6
55	F	E	W	P	N	F	K	Y	92 ± 3
56	F	E	W	L	N	W	K	Y	3.2 ± 1.0
57	F	E	W	L	N	H	K	Y	24 ± 1
58	F	E	W	D	Q	F	K	Y	7.2 ± 1.3
59	F	E	W	D	Q	F	P	I	32 ± 1.4
60	F	D	W	L	N	F	K	Y	11.3 ± 2.4
61	F	Q	W	L	N	F	K	Y	17.3 ± 4.1
62	F	E	W	L	N	F	R	Y	7.7 ± 0.2
63	F	E	W	L	N	F	E	Y	5.9 ± 0.1
64	F	E	W	L	N	F	Q	Y	3.5 ± 0.1
65	F	Q	W	L	N	F	Q	Y	12.3 ± 1.9
66	F	D	W	L	N	F	Q	Y	9.7 ± 0.3
67	F	E	W	L	N	W	E	F	0.89 ± 0.05

Table 2. (Continued)

Mimetic	1	2	3	4	5	6	7	8	IC <sub>50</sub> [μM]
68	F	D	W	L	N	F	E	Y	14.4 ± 0.14
69	F	E	W	L	N	W	E	Y	1.4 ± 0.28
70	F	E	W	NIP	N	F	E	Y	2.6 ± 0.56
71	F	E	W	L	D	W	E	F	0.54 ± 0.06
72	F	E	W	D	Q	W	E	F	1.3 ± 0.2
73	F	E	W	NIB	D	W	E	F	0.37 ± 0.08
74	Bip	E	W	L	D	W	E	F	3.7 ± 0.63
75	F	E	Bip	L	D	W	E	F	1.6 ± 0.32
76	F	E	w	L	N	W	E	F	28 ± 2.6
77A	F	E	<sup>(6Cl)</sup> W	L	N	W	E	F	0.52 ± 0.01
77B	F	E	<sup>(6Cl)</sup> W	L	N	W	E	F	2.5 ± 0.14
78A (2) <sup>[a]</sup>	F	E	<sup>(6Cl)</sup> W	L	D	W	E	F	0.14 ± 0.07
78B	F	E	<sup>(6Cl)</sup> W	L	D	W	E	F	0.68 ± 0.14

[a] Mimetic **78A** is identical to **2** in Figure 1B. The standard single letter code is used for proteinogenic amino acids. w = D-tryptophan, <sup>(6Cl)</sup>W = D- or L-6-chlorotryptophan, NIP = N-(3-methylbutyl)glycine (N-isopentylglycine), NIB = N-(2-methylpropyl)glycine (N-isobutyl)glycine Bip = L-biphenylalanine. The absolute configuration of <sup>(6Cl)</sup>W in **78A** is L, from the crystal structure, so that in **77A** can also be inferred to be L. [b] Estimation of IC<sub>50</sub> was limited by the poor solubility of the mimetic.

served, suggesting slow interconversion between multiple backbone conformations. The disulfide-bridged mimetic **24** showed weaker activity than **1**. At this point, further improvements in the inhibitory activity were found by pursuing other leads.

One lead (**25**), with Tyr at position 5, showed a twofold increase in affinity towards HDM2 relative to **1**. A new sublibrary was designed (mimetics **25–41**, Table 2) with the sequence of **25** as a starting point. The residues at positions 1, 3, and 6 were generally held constant or were substituted with other aromatic/hydrophobic amino acids. To enhance water solubility, positions 2 and 7 were exploited to introduce charged/polar residues. Some members of the library were designed to explore the effects of substitutions in the loop region, in particular, β-turn sequences that enhance β-hairpin formation, such as Asn–Gly at the *i*+1 and *i*+2 positions.<sup>[27–29]</sup> Attempts were also made to exploit hydrophobic interactions further through the introduction of aromatic residues in position 8.

The inhibitory activities revealed that the introduction of an aromatic residue at position 8 (**28**) enhanced binding to HDM2 fivefold in relation to mimetics **25** and **27**, and tenfold in relation to **26**. The residue 8 binding site on HDM2 revealed a preference for Phe > Tyr ≫ Bip (=L-biphenylalanine; **28**, **29**, **30**). A similar trend (Phe > Bip > Tyr; **31**, **26**, **32**) could also be observed for position 6 in this series of mimetics. On the other hand, none of the substitutions made in the loop residues produced any significant improvements in activity, including the Asn–Gly pair (e.g., **28** vs. **38**). Curiously, replacement of either Phe1 or Trp3 with Bip (**39** and **40**) was well tolerated, whereas exchanging Phe and Trp at positions 1 and 3 (**41**) caused a large drop in activity. These results confirm that a suitable orientation of these key aromatic residues is important for HDM2-binding activity.

Next, several of the substitutions that individually gave enhanced inhibitory activity were combined in a new series of

mimetics (42–69). A subseries (42–50) based on the most active compound from the first sublibrary (10) was designed, whilst a second subseries (51–69) was based on mimetics 28 and 29. Aromatic amino acids were tested in positions 6 and 8, to explore the properties of the cognate binding pockets on the protein further. Positions 2 and 7 were generally charged residues, the aim being to aid the solubility of otherwise rather hydrophobic peptides. Among the peptides based on 10 (Table 2, 42–50), no further gain in activity was achieved.

In contrast, about 50% of the compounds from the second sublibrary (51–69) were shown to bind HDM2 more tightly than the parent compounds ( $IC_{50} < 10 \mu\text{M}$ ), and in only three cases did the activity drop by more than twofold. Pairwise comparisons yielded some valuable insights into structure–activity relationships within this group of mimetics. The preference at position 8, for example, was Phe > Tyr > Trp, whilst that at position 6 was Trp > Phe > Tyr. The preferences at positions 2 and 7 were Glu  $\approx$  Leu > Lys  $\approx$  Asp > Gln in the former, and Gln > Glu  $\approx$  Arg > Lys in the latter. In one peptide, mimetic 67, the combination of multiple beneficial replacements gave an affinity improvement of about tenfold over the starting compounds. With an  $IC_{50}$  of 0.89  $\mu\text{M}$ , mimetic 67 showed an affinity to HDM2 comparable to that of the natural substrate (5,  $IC_{50} = 1.1 \mu\text{M}$ ). Hence, an effective  $\beta$ -hairpin mimetic of the p53 peptide had at this point been identified.

In further efforts to improve the HDM2-binding properties (Table 1, 70–78B), a peptoid unit was introduced at the hairpin tip (70, NIP = *N*-isopentylglycine [*N*-(3-methylbutyl)glycine]),<sup>[30]</sup> *N*-Methyl amino acids and peptoid units at the *i*+1 position are known to stabilize  $\beta$ -turn conformations,<sup>[31,32]</sup> and this has been exploited to stabilize hairpin conformations in a protegrin mimetic.<sup>[14]</sup> Mimetic 70 showed an affinity improved by about twofold (compare 63). NMR studies on 70, reported earlier,<sup>[15]</sup> clearly revealed a stable and regular  $\beta$ -hairpin conformation for this mimetic in MeOH/water (1:1) solution; this suggests that the  $\beta$ -hairpin scaffold should present the key hot residues in the desired geometry for binding to HDM2.

Further small gains in inhibitory activity came through the introduction of Asp at position 5 (71 vs. 67), and upon replacing Trp3 with 6-chlorotryptophan ((6-Cl)Trp) (67 vs. 77A). Earlier studies on a p53-derived linear peptide by Garcia-Echeverria and co-workers had shown that a Trp23 to (6-Cl)Trp substitution gave rise to a 60-fold increase in affinity for HDM2.<sup>[33]</sup> Here, racemic DL-6-chlorotryptophan was incorporated at position 3 and the resulting diastereomers were separated by HPLC (denoted in Table 2 as A and B). Only in the case of mimetic 78A was the absolute configuration verified by X-ray crystallography (see below). The importance of the configuration of Trp3 in mimetic 67 is indicated by the much weaker affinity of mimetic 76, containing D-Trp3.

The substitutions of Asn5 for Asp (71) and of Trp3 for (6-Cl)Trp (77A) both improved the affinity of mimetic 67. The combination of these two modifications caused an additive enhancement of the peptide inhibitory activity ( $IC_{50} = 140 \text{ nM}$ ), leading to the most active HDM2 inhibitor (mimetic 78A, identical to 2 in Figure 1) discovered in this work.

#### 4. Further conformational and chemical shift mapping studies

NMR conformational studies on mimetic 63 were performed in DMSO, due to its low solubility in water at pH < 7. Also, the observation of concentration-dependent changes in linewidths and chemical shifts suggested that the mimetic may aggregate at mM concentrations in water. Mimetic 63 was selected for conformational studies as a representative of the subset of mimetics showing low  $\mu\text{M}$  affinity to HDM2. The 1D  $^1\text{H}$  NMR spectrum of 63 showed a single average conformer in solution on the NMR timescale, with all peptide bonds *trans*, as found for 1. In mimetic 63, the aromatic side chains are connected by a large number of medium- and long-range ROEs. Cross-strand ROE connectivities between the NH protons of Phe1 and Tyr8, as well as those of Trp3 and Phe6, and between the C( $\alpha$ )H protons of Glu2 and Glu7 are observed, strongly supporting the presence of a regular  $\beta$ -hairpin conformation in DMSO. Several large (> 8 Hz)  $^3J_{\text{HN,H}\alpha}$  coupling constants are also seen for both 63 and 70, which provide further evidence for regular  $\beta$ -structure.

Average NMR structures calculated for 63 revealed convergence to a well defined 2:2  $\beta$ -hairpin conformation with a type II  $\beta$ -turn at Leu4/Asn5 (Figure 2 and Table 1). The side chains of Phe1, Trp3, Phe6, and Tyr8 now form a hydrophobic core clustering on one side of the hairpin. The side chain of Leu4 lies in close proximity to the indole ring of Trp3, which in turn T-stacks with the side chain of Phe6, forming a hydrophobic cluster that probably stabilizes a regular  $\beta$ -hairpin fold. In mimetic 1, which lacks an aromatic side chain at position 6, Trp3 was found to pack together with Phe1 and Leu4, inducing a profound distortion of the peptide backbone (Figure 2). The proline ring of  $\text{L-Pro10}$  in 63 also seems to participate in the cluster, packing against the benzene ring of Phe1, which may represent a structure-stabilizing motif common to this family of molecules.

Chemical shift mapping with  $^{15}\text{N}$ -labeled HDM2 was again used to confirm that the optimized ligands interact specifically with the p53-binding site. To facilitate the assignment of chemical shift perturbations, the peptide was titrated into  $^{15}\text{N}$ -labeled protein at protein-to-peptide ratios of 4:1, 2:1, 1:1, and 1:2. In contrast to the other mimetics, the HDM2/78A complex was found to exist in slow exchange on the NMR timescale (at 600 MHz and 900 MHz) giving rise, in the presence of substoichiometric amounts of ligand, to two sets of cross peaks corresponding to free and ligand-bound  $^{15}\text{N}$ -labeled protein. Upon titration of  $^{15}\text{N}$ -labeled HDM2 with 78A, many amide resonances of residues surrounding the binding cleft exhibited large ligand-induced shifts (see Supporting Information). Other more remote amide NHs were also significantly affected, including residues lying on the  $\alpha$ 1-helix,  $\beta$ 2-strand, and the  $\alpha$ 1'-helix.

#### 5. Crystal structure of the HDM2/78A complex

In order to crystallize the HDM2/78A complex, the His<sub>6</sub>-tag was removed from the fusion protein by thrombin digestion. The 1.40 Å resolution crystal structure of the resulting HDM2/

**78A** complex (see Table 3 and Figure 3) confirmed the regular 2:2  $\beta$ -hairpin conformation of bound mimetic **78A** (Figure 4) and the amphipathic character of the ligand. Mimetic **78A** binds to HDM2 mainly through interactions involving aromatic

**Table 3.** Crystal structure—data collection and refinement.

Data collection	
X-ray source	Swiss Light Source
wavelength [Å]	0.91913
unit cell [Å]	45.21, 77.78, 61.25
resolution <sup>[a]</sup> [Å]	1.40 (1.40–1.48)
completeness <sup>[a]</sup> [%]	96.4 (95.4)
$R_{\text{sym}}$ <sup>[a]</sup> [%]	4.8 (38.0)
redundancy	4.0 (4.0)
$R_{\text{merge}}$ <sup>[b]</sup> [%]	14.3
reflections [ $I > 4\sigma$ ]	19289 (15759)
refinement	
resolution [Å]	40–1.40
$R_f$ [%]	14.90 (13.76)
$R_{\text{free}}$ [%]	23.36 (22.37)
no. of atoms	984
$\text{rm}_{\text{sbond}}$ [Å]	0.011
$\text{rms}_{\text{angle}}$	2.3°

[a] Values in parentheses refer to the highest-resolution shell. [b] Data in the resolution range 40 to 3.0 Å

groups. The side chains of the hydrophobic residues Phe1, (6-Cl)Trp3, Leu4, Trp6, and Phe8 face HDM2, while the side chains of Glu2 and Glu7 point towards the solvent (Figure 3). The side chain of Asp5 at the tip of the hairpin interacts with the N-terminal tail of HDM2 (*vide infra*). As expected, binding of **78A** places residues Phe1, (6-Cl)Trp3, and Leu4 in the hydrophobic p53-binding cleft on the surface of HDM2, burying surface areas of approximately 550 Å<sup>2</sup> and 510 Å<sup>2</sup> on HDM2 and **78A**, respectively. The residue Leu4 in bound **78A** is located in a disallowed region of the Ramachandran diagram ( $\phi = +50^\circ$ ,  $\psi = -125^\circ$ ) as part of a type II'  $\beta$ -turn. The interactions between **78A** and HDM2 were investigated by the shape complementarity method developed by Lawrence and Colman.<sup>[34]</sup> A statistical value of 0.75 indicates that **78A** fits the HDM2 p53-bind-

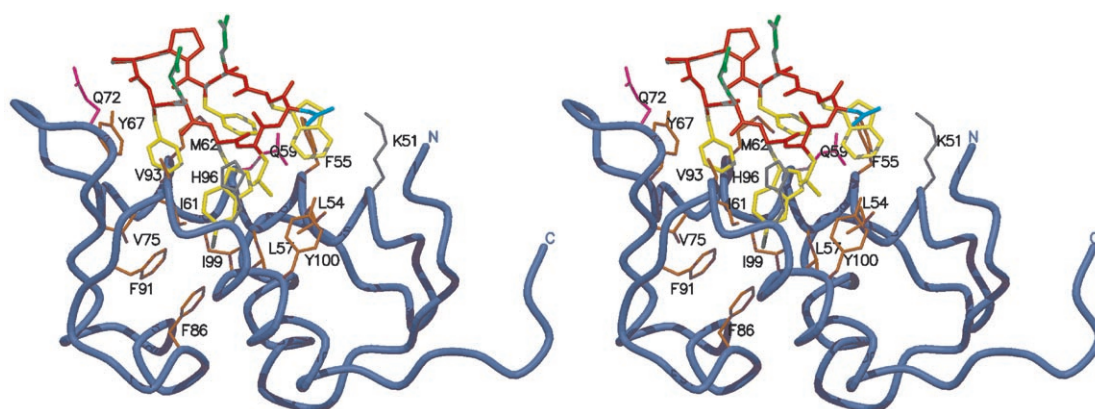


**Figure 3.** Stereo representation of the 1.4 Å crystal structure of HDM2 complexed to the inhibitor **78A** (= **2**; backbone in red, side chains in yellow (aromatic/hydrophobic), green (Glu2/Glu7), and cyan (Asp5)). The N and C termini of HDM2 are labeled. Side chains in HDM2 that are in, or close to, the p53 binding site are shown with colored sticks.

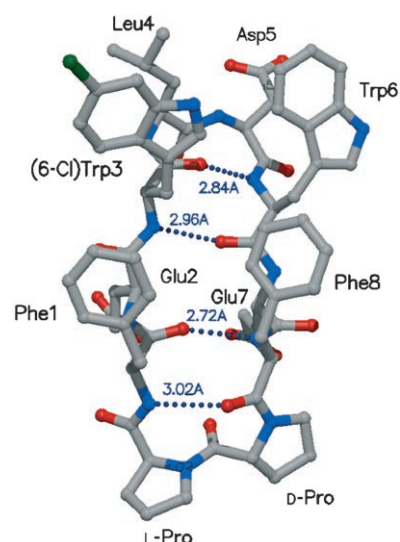


**Figure 4.** The conformation of ligand **78A** (= **2**) bound to HDM2. Cross-hairpin hydrogen bonds are shown. O atoms in red, N atoms in blue, Cl atom in green. The D-Pro-L-Pro template is at the bottom.

ing site as well as the natural ligand (sc value of 0.76; Figure 5).

A structural adaptation of HDM2 to the inhibitor **78A** (relative to the p53/HDM2 complex) is indicated by the rmsd of 0.9 Å for superposition of the HDM2 backbone atoms in this complex with those in the crystallographically determined HDM2/p53 complex (PDB file 1YCR). Although the 1YCR structure was determined at significantly lower resolution (2.6 Å vs. 1.4 Å for the HDM2/**78A** complex), a general contraction of the p53-binding pocket in the HDM2/**78A** complex is apparent. The distances between the C $\alpha$  atoms of Phe55 and Tyr100, which are located in the  $\alpha$ -helices on opposite sides of the p53-binding pocket, are more than 1 Å shorter in the HDM2/**78A** complex than in the HDM2/p53 complex (Figure 6).

The side chain of (6-Cl)Trp3 penetrates deep into the p53/Trp23 binding pocket of HDM2 and places the chlorine atom at an interaction distance of 3.4 Å from the edge of the ar-

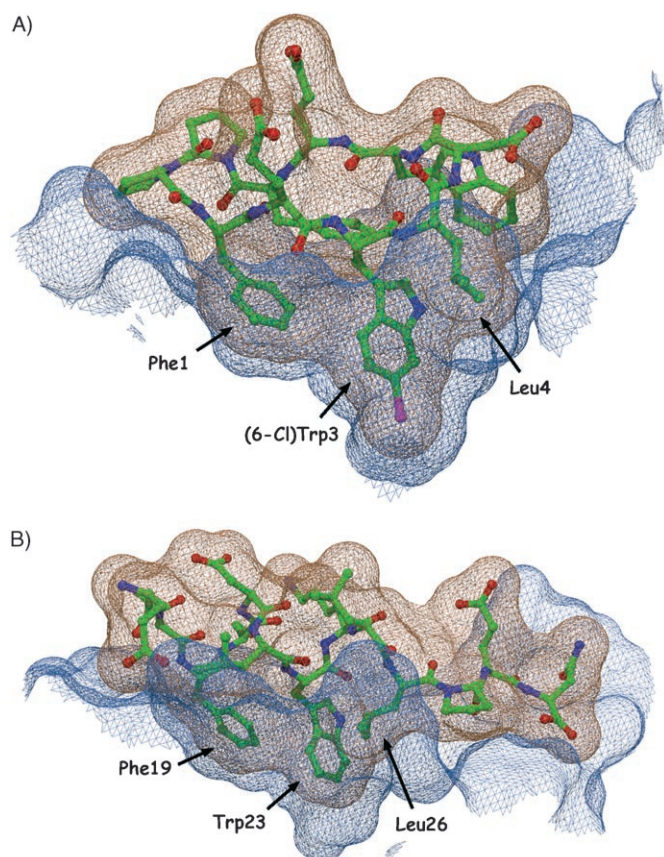


**Figure 5.** Protein–ligand surface complementarities shown for A) the HDM2/78A complex and B) the HDM2/p53 complex. The surface of HDM2 is in blue, and those of the ligands are in brown. Stick model of the ligands (green/red/blue) are also visible.

matic side chain of Phe86 (Figure 7). The location of the chlorine atom was confirmed in an anomalous difference electron density map (data not shown). Despite its aromatic character,

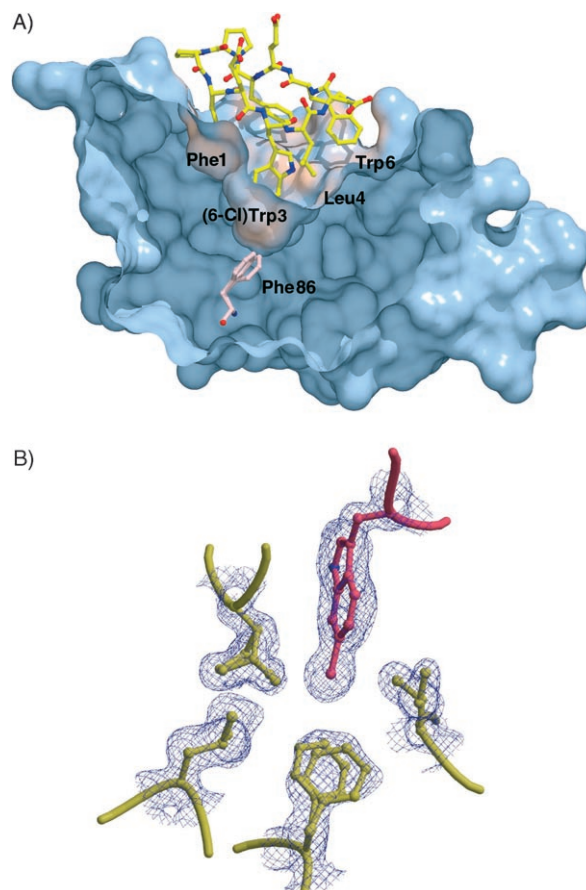


**Figure 7.** A) Surface representation of the HDM2/78A complex, with the ligand 78A (=2) shown as a stick model. A slice through the surface of the HDM2/2 complex is shown with the binding pockets for Phe1, (6-Cl)Trp3, and Leu4 in 78A and the alternate side-chain conformations detected for Phe86 in HDM2. B) Electron density in the core of the complex, showing the 6-chlorotryptophan side chain (red) in 78A, and side chains of HDM2 (yellow). The 2Fo-Fc map was contoured at 1.1  $\sigma$ . Alternative side-chain conformations are shown for Phe86 and Leu57 in HDM2.

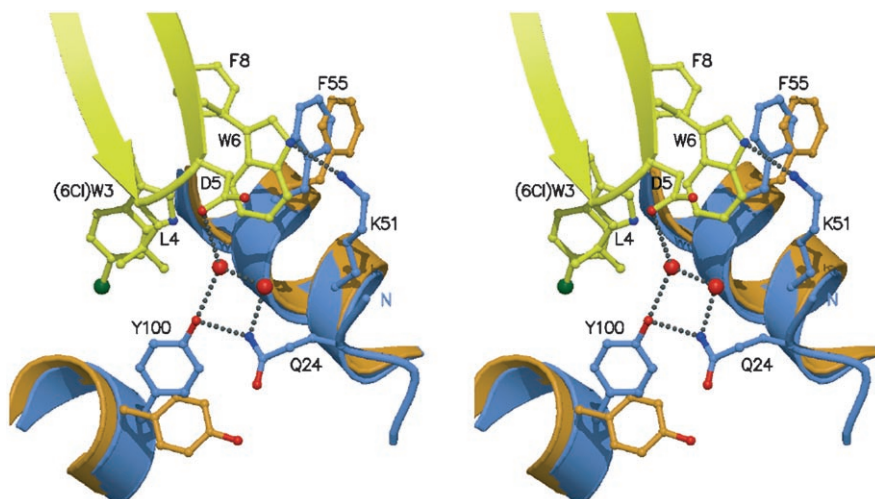


**Figure 6.** Interactions between 78A (yellow), HDM2 (blue), and two crystallographically determined water molecules (red balls). The positions of the same parts of the HDM2 protein taken from its complex with p53 (PDB file 1YCR, orange) are also shown, including the alternate side-chain conformations of Phe55 and Tyr100 in the two complexes, as well as the contraction of the ligand-binding site (shortening of the Phe55–Tyr100 distance, see text).

the 6-chloroindole ring system appears to be slightly bent, by more than 0.1 Å, as indicated by strong difference electron density that appears if the default values for planarity restraints are used. Interestingly, the refined HDM2/78A structure reveals alternative conformations for the side chains of Phe86 and Leu57, which are buried in the core of the protein (Figure 7). In addition, the side chain of Phe86 has changed its position in relation both to the HDM2/p53 and to the recently disclosed<sup>[35]</sup> HDM2/nutlin-2 complexes (vide infra), because of the close interaction distance with the chlorine atom of (6-Cl)Trp3.

The crystal structure of the HDM2/**78A** complex also reveals important contacts—not envisaged in the initial design of the ligand—between HDM2 and **78A**. Thus, apart from the designed contacts to HDM2 involving Phe1, (6-Cl)Trp3, and Leu4, the side chains of Trp6 and Phe8 in the second  $\beta$ -strand stack on both sides of Phe55 in the second HDM2  $\alpha$ -helix (Figure 6 and Figure 8). The edge of the phenyl ring in Phe55 T-stacks onto the face of the indole in Trp6, while at the same time the

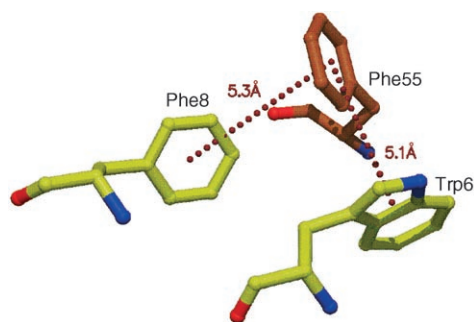


**Figure 8.** The aromatic–aromatic stacking interactions involving the Phe55 side chain (orange) in HDM2 and Trp6 and Phe8 in **78A** (yellow).

face of Phe55 T-stacks with the edge of the phenyl ring of Phe8 in **78A**. These stacking interactions are not seen in the HDM2/p53 complex, in which the Phe55 side chain is rotated slightly away from the ligand-binding pocket into solution (Figure 6). The Tyr100 side chain has also rotated, by around  $120^\circ$  compared to its conformation in the HDM2/p53 complex.

In the HDM2/**78A** complex, only two protein–ligand hydrogen bonds were observed: between (6-Cl)Trp3-NE1 and Leu54-O (2.74 Å) and Trp6-NE1 and Lys51-NZ (3.30 Å). Interactions were also observed between the Asp5 side chain of **78A** and both the N terminus of HDM2 and the positive surface potential caused by Lys51 (Figure 3). The Asp5 side chain also forms water-mediated hydrogen bonds with the side chains of Tyr100 and Gln24 (Figure 6). In the p53/HDM2 complex, hydrogen bonding interactions are apparent between Phe19-N and O( $\gamma$ )-Gln72 [3.02 Å (O to N)], Trp23-NE1 and O-Leu54 [2.8 Å (O to N)], and two hydrogen bonds between Asn29-O and Tyr100-OH [2.7 and 2.8 Å (O to O)].

## Discussion

The starting point for the design of the peptidomimetics reported in this paper was the crystal structure of a p53-derived peptide in complexation with the p53-binding domain of HDM2 (PDB file 1YCR).<sup>[17]</sup> This revealed a helical conformation for the HDM2-bound p53-peptide. The aim here was to mimic the spatial arrangement of key groups along one face of the p53 helix through use of a  $\beta$ -hairpin scaffold. Through a series of optimization steps, the inhibitory activity of the initial lead (**1**) was improved by a factor of almost 1000 to give the mimetic **2** (**78A** in the list of mimetics in Table 2).

The crystal structure of the HDM2/**78A** complex confirms the regular 2:2  $\beta$ -hairpin geometry of the bound inhibitor and

documents several small changes in the structure of HDM2 in relation to that in the p53/HDM2 complex (Figure 6 and Figure 7). These involve several side-chain conformational changes, as well as small movements of major secondary structural elements. In particular, a contraction of the binding pocket due to a slight movement of the  $\alpha$ -helices on opposite sides of the binding cleft is apparent (Figure 6). Recently, a new NMR structure of the corresponding ligand-free HDM2 protein (called MDM2 in ref. [36]) was published. This is of special interest here, since the NMR structure suggests that these helices are even closer together (3–4 Å) in the free protein than is seen in the complex with p53. The extent to which HDM2 exists as a dynamic ensemble of conformations in solution is still uncertain, but the surface of the protein certainly appears to adapt significantly to the ligand **78A** through an induced-fit mechanism of binding.

It is of particular interest to understand the origins of the 1000-fold improvement in activity observed on going from **1** to **78A**. NMR studies on the initial lead mimetic **1** indicate that a regular 2:2  $\beta$ -hairpin conformation (compare Figure 1B) is not significantly populated in aqueous solution (Figure 2). This is important, since the conformation of **1** would not then display the three key side chains (Phe1, Trp3, and Leu4) in the optimal spatial orientation for binding to HDM2. This may well contribute to the low affinity of **1** for HDM2. In contrast, the calculated average NMR solution structures of **63** and **70** (albeit determined in the presence of organic solvents) reveal regular 2:2  $\beta$ -hairpin conformations very similar to that of **78A** in the crystal structure with HDM2. Improved mimicry of a regular  $\beta$ -hairpin structure in the free ligand should energetically favor recognition and binding to HDM2.

The HDM2/**78A** crystal structure reveals contacts between **78A** and HDM2, not seen in complexes of HDM2 with p53 or several other recently reported small-molecule inhibitors (see below), which are exploited by the  $\beta$ -hairpin to achieve high affinity binding. These involve the side chains of Trp6 and Phe8, as well as Asp5 in the inhibitor. The SAR studies showed how the activity improves significantly when aromatic groups are introduced at positions 6 and 8 in the  $\beta$ -hairpin mimetic, with preferences for Trp  $\gg$  Phe  $>$  Tyr at position 6 and Phe  $\gg$  Tyr  $>$  Trp at position 8 (Table 2). These preferences indicate differences in the size and/or properties of the corresponding binding pockets on the surface of HDM2. The origins of these effects become clear upon analysis of the crystal structure, in which the side chains of Trp6 and Phe8 are seen to participate in a small network of stacking interactions with Phe55 on HDM2 (Figure 8). It is well appreciated that individual aromatic–aromatic stacking interactions can have a significant influence on protein stability.<sup>[37–39]</sup> No comparable interactions are seen between p53 and HDM2 in their complex, where the Phe55 side chain rotates away and does not come into contact with the peptide ligand.

A significant contribution to binding energy is also made by the side chain of Asp5 in **78A**, which interacts with the N-terminal region of HDM2 (Table 2, Figure 6). McCoy et al.<sup>[40]</sup> postulated that the N-terminal tail of HDM2 may serve as a lid by folding back and covering the rather hydrophobic p53 binding

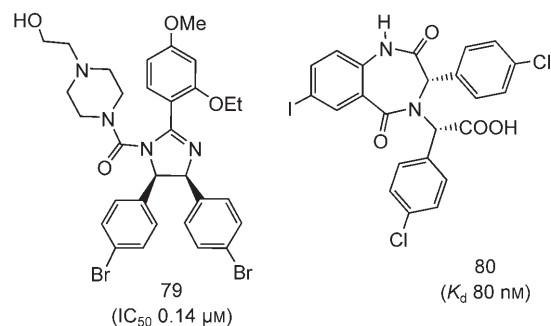


site, and proposed that docking of p53 is associated with the displacement of this lid from the binding site. The recently reported NMR structure of ligand-free HDM2 also concluded that p53 effects displacement of an N-terminal segment of apo-HDM2 that occludes access to the shallow end of the p53-binding cleft.<sup>[36]</sup> In the complex with **78A**, it appears that the lid also adapts to the size of the ligand through a conformational rearrangement (**78A** occupies only the central part of the cleft defined by p53) and may even act to stabilize the complex. By rotating  $\chi_1$  by ca.  $120^\circ$  relative to its conformation in the HDM2/p53 complex, the Tyr100 side chain also acts to limit the length of the p53-binding groove (Figure 6).

The noncovalent interaction between the halogen in **78A** and the aromatic ring of Phe86 is also of interest. The energies of such interactions are so far not well characterized. A recent model study suggested that interaction of a chlorine atom with the face of an aromatic ring is energetically unfavorable.<sup>[41]</sup> It is well known that positively charged ammonium groups interact favorably with the  $\pi$ -electron clouds of aromatic rings through van der Waals contacts, and are therefore frequently seen above or below the planes of aromatic rings in protein crystal structures.<sup>[42,43]</sup> Partial negatively charged species should interact preferentially with the aromatic hydrogens in the  $\sigma$ -skeleton, which carry partial positive charges, as seen in this complex. In contrast, several examples of aromatic–Cl bonds pointing toward the faces of aromatic rings in tyrosine residues are known in serine protease–inhibitor complexes.<sup>[44–48]</sup> Moreover, such interactions apparently occur quite frequently in small-molecule crystal structures.<sup>[45]</sup> However, the magnitude of any electrostatic interaction could be very sensitive to the distance between the Cl atom and the aromatic ring. Apart from electrostatic effects, the increase in hydrophobicity arising from the introduction of a chlorine atom at C6 in the indole ring of **78A** should also favor binding in the hydrophobic pocket on HDM2.<sup>[49]</sup> In practice, replacing a Trp3 residue by (6-Cl)Trp3 caused an almost fourfold increase in inhibitory activity (Table 2, **71** vs. **78A**). For comparison, Garcia-Echeverria et al.<sup>[33]</sup> reported that the affinity of a linear octapeptide p53/HDM2 inhibitor to HDM2 was increased by a factor of over 60 after such a Trp to (6-Cl)Trp substitution. No 3D structure for this linear peptide/HDM2 complex is available, but the much larger effect on binding reflects the different sums of interactions that each inhibitor makes in their respective complexes with HDM2.

It is appropriate here to compare these results with those gained with other recently discovered p53/HDM2 inhibitors. Known inhibitors include the natural product chlorofusin,<sup>[50,51]</sup> various linear  $\alpha$ -peptides,<sup>[33,52–60]</sup>  $\beta$ -peptides,<sup>[61,62]</sup> and some chalcone derivatives.<sup>[63,64]</sup> More recently, a series of *cis*-imidazolines,<sup>[35]</sup> isoindolinones,<sup>[65]</sup> 1,4-benzodiazepinediones,<sup>[60,66]</sup> terphenyls,<sup>[67,68]</sup> and a sulfonamide<sup>[69]</sup> that inhibit the binding of p53 to HDM2 have also been described.

Crystal structures of one *cis*-imidazoline (nutlin-2, **79**, PDB 1RV1) and a benzodiazepinedione (**80**, PDB 1T4E), each in complexation with HDM2, confirmed that these ligands also occupy the p53-binding site. Compound **79** binds to HDM2 with an affinity ( $IC_{50} = 140$  nM) similar to that of **78A**, with one



bromophenyl moiety sitting in the Trp pocket, the other occupying the Leu pocket, and the ethyl ether side chain directed towards the Phe pocket. Compound **80** also has a similar affinity ( $K_d = 80$  nM), the two chlorophenyl moieties now interacting with the Trp and Leu pockets and the iodo substituent pointing into the Phe pocket. With both **79** and **80** the interactions with HDM2 are largely nonspecific hydrophobic van der Waals contacts. However, the mechanism of **78A** binding to HDM2 is clearly different to the extent that not only the Phe/Trp/Leu trio of side chains interact with their cognate pockets on HDM2, but new aromatic–aromatic T-stacking contacts are also made with Phe55 in  $\alpha$ -helix2.

Several of the small-molecule inhibitors have been shown to activate p53 on whole cells,<sup>[35,60,68]</sup> indicating that they are cell-permeable and can interact with HDM2 within cells. Cellular uptake is an important property and it remains to be seen whether the  $\beta$ -hairpin mimetics reported here can permeate cell membranes, or whether this property can be optimized in this family of molecules by further modification of the hairpin scaffold. Another relevant question concerns the specificity of the inhibitors for HDM2. Here the  $\beta$ -hairpin PEM approach may offer some advantages, since the small-molecule inhibitors **79** and **80** mimic p53 by targeting only the large hydrophobic cleft on HDM2. We have shown that **78A** achieves high binding affinity to HDM2 by also exploiting specific stacking interactions with HDM2 that do not form part of the p53 binding cavity. At present, however, no experimental data are available to indicate how specific the PEM-based inhibitors are for HDM2.

## Conclusion

To conclude, this work demonstrates that  $\beta$ -hairpin PEMs can be designed to mimic an  $\alpha$ -helical epitope, and that the hairpin represents a convenient scaffold to display hot spot residues in a defined array for interaction with a protein surface. It may be argued that this p53–HDM2 example is a special case, since many protein–protein interactions are not characterized by such an extensive hydrophobic ligand-binding pocket as seen on HDM2. It is certainly encouraging to see here how the optimization of ligand **78A** exploits binding contacts to groups on HDM2 not used by the natural ligand p53. It may be possible to exploit this feature in the discovery of other interesting PEM-based protein–protein interaction inhibitors.

## Experimental Section

**Production of HDM2(17–125):** DNA encoding residues Ser17 to Asn125 of HDM2 was cloned as a *NdeI/BamHI* fragment into pET14b (Novagen). Recombinant clones carrying the correct insert were identified by DNA sequencing. Plasmid from these clones was introduced into *E. coli* BL21(DE3)pLysS and protein production in LB medium was induced with IPTG (1 mM) when the cell density reached  $OD_{600} = 1.1$ . Induced cells were grown at 24 °C for 5 h, harvested, and then resuspended in buffer A [TrisHCl (20 mM), NaCl (300 mM), imidazole (20 mM), pH 7.9]. After cell disruption and centrifugation, supernatant (containing 5–20 mg protein) was loaded onto a Ni-nitrilotriacetic acid (NTA) column and His<sub>6</sub>-tagged HDM2(17–125) was eluted with buffer A containing imidazole (300 mM). The protein was further purified by cation-exchange chromatography [Pharmacia Mono S 5/5, 1 mL min<sup>-1</sup>, sodium phosphate (25 mM), EDTA (1 mM), DTT (1 mM), pH 6.7] with a 0–1.0 M NaCl gradient. The HDM2(17–125) eluted in two fractions, at 220 mM, corresponding to monoacetylated protein (ESI-MS  $[M+Ac+H]^+$   $m/z$  14861.6 ± 1; calc: 14856.5), and at 280 mM NaCl, corresponding to protein lacking the N-terminal methionine (ESI-MS  $[M-Met+H]^+$   $m/z$  14683.0 ± 1; calc: 14683.2). The two fractions showed the same binding affinity to **3** in a direct BIAcore binding assay. The expression yield was ~9 mg L<sup>-1</sup> culture.

**BIAcore assays:** All measurements were carried out on a BIAcore 1000 instrument at 25 °C with HBS as running buffer [HEPES (10 mM), NaCl (150 mM), EDTA (3.4 mM), surfactant p20 (0.005%), pH 7.4]. The biotinylated p53-derived peptide (**3**) was captured on a SA sensor chip at a density of 570–600 RU. An untreated flow cell was used as reference surface to correct for bulk refractive index changes. A solution of His<sub>6</sub>-tagged HDM2(17–125) protein (0.250 μM) in HBS was incubated with increasing amounts of inhibitor, and this solution (20 μL) was injected over the specific and reference surfaces at a flow rate of 10 μL min<sup>-1</sup>. A blank injection with buffer was also included. Two minutes after the end of the injection, the remaining surface-bound protein was completely removed with a 30 s pulse of HCl (10 mM). Specific binding curves for each concentration of inhibitor were obtained by subtracting the response in the reference surface from the response in the p53-coated surface. Response values were calculated by averaging the last 10 s of each sample injection. Inhibition curves were obtained by plotting the decrease in binding response against the increase in the inhibitor concentration. For each inhibitor, seven different concentrations were used and each solution was injected twice. IC<sub>50</sub> values were calculated from the inhibition curves. The reported mean values and standard deviations derive from at least three independent experiments (Table 2). An internal standard (peptide **5**) was included in each experiment to verify the reproducibility of the assay.

**Crystallization, structure solution, and refinement:** His<sub>6</sub>-tagged HDM2(17–125) protein was digested with thrombin (Roche; 0.07 U per mg protein) for 2.5 h. Prior to digestion the protein was dialyzed against thrombin cleavage buffer. After the enzymatic reaction, the digested protein was purified by cation-exchange chromatography, as described above. From the Mono-S column a protein with the expected size by SDS-PAGE was eluted as single peak at 110 mM NaCl. The protein was further purified by gel filtration chromatography on a Superdex-75 column (Pharmacia) equilibrated with MES (20 mM), NaCl (250 mM), DTT (5 mM), pH 6.8; by ESI-MS  $m/z$  12933.1  $[M+H]^+$  (expected 12932.7 g mol<sup>-1</sup>); N-terminal Edman sequencing showed the expected sequence (GSHMSQ...). The HDM2/**78A** complex was prepared by mixing a 2:1 molar ratio of peptide:HDM2 and concentrating the mixture to a final concen-

tration of 1 mM HDM2. Initial screening for crystallization conditions was performed in 96-well plates with a robotic system (Tecan). Small crystals with a plate-like morphology (10–15 μm long) were observed in MES (100 mM), ammonium sulfate (50% sat.), pH 6.0. Refinement of crystallization conditions was performed in 24-well hanging-drop plates. Larger crystals (210 × 150 × 30 μm<sup>3</sup>) were obtained by applying the micro-seeding technique with use of a 1:1 mixture of HDM2/**78A** complex with MES (100 mM), ammonium sulfate (44% sat.), pH 5.5.

X-ray diffraction data were collected on a rotating anode X-ray generator (Bruker, FR591) fitted with Osmic mirrors and a Mar345 image plate detector system, and on a synchrotron X-ray source fitted with a MarCCD detector (Swiss Light Source, Würenlingen). X-ray diffraction data were processed with XDS.<sup>[70]</sup> Data sets were merged to replace saturated reflections at low resolution in the high-resolution data set. Crystals belonged to space group C222<sub>1</sub> with one molecule per asymmetric unit. Molecular replacement (AMORE program<sup>[71]</sup>) using data in the 40 to 3.0 Å resolution range and the HDM2 coordinates from the HDM2/p53(15–29) crystal structure (pdb-code: 1YCR) yielded significant solutions. The correctly positioned search model was refined to 1.9 Å resolution with the program REFMAC.<sup>[72]</sup> During the final stages alternative side-chain conformations, anisotropic B-factors, and hydrogen atoms at C<sub>α</sub>-atoms were included in the refinement (program SHELXL<sup>[73]</sup>). The final map clearly showed electron density for all main chain atoms from residues 23 to 114, the inhibitor **2**, 96 water molecules, two sulfate ions, and one 3-morpholinopropanesulfonic acid molecule. Alternative conformations have been included for residues 29, 35, 39, 46, 57, 63, 76, 81, and 86. Surface complementarity was investigated with the SC program from the CCP4 program suite with use of the default parameters. The buried surface area was calculated with GRASP<sup>[74]</sup> by subtraction of the accessible surface area of the whole complex from the sum of the accessible surface areas of the isolated molecules with use of a probe radius of 1.4 Å. Figure were prepared by use of the programs MOLMOL,<sup>[75]</sup> Pymol (<http://www.pymol.org>), and Bobsript.<sup>[76]</sup>

The crystal structure has been deposited at the Protein Data Bank under the accession number 2AXI.

**Synthesis:** The peptidomimetics were made by parallel synthesis on a Syro-II (Microsyntec, Germany) peptide synthesizer typically with use of 12–24 reaction vessels, by a method described earlier.<sup>[9]</sup> Each mimetic was purified by reversed-phase HPLC-MS (C18 column, gradient from 5–95% MeCN/H<sub>2</sub>O + 0.1% TFA). For analysis of each purified product (C18 column, flow 1 mL min<sup>-1</sup>, gradient from 5–95% MeCN/H<sub>2</sub>O + 0.1% TFA over 20 min) the HPLC instrument was interfaced with a Finnigan AQA electrospray ionization (ESI) mass spectrometer (MS). The ESI-MS of all mimetics in every case confirmed the expected molecular weight (see Supplementary Information). The purities of all mimetics were >95% as analyzed by two independent methods: reversed-phase HPLC (C18 column, flow 1 mL min<sup>-1</sup>, gradient from 5–95% MeCN/H<sub>2</sub>O + 0.1% TFA over 20 min) and high-field <sup>1</sup>H NMR spectroscopy (600 MHz).

**NMR studies:** Structure calculations performed on **1** and **63** with the available ROE and dihedral angle restraints gave low-energy DYANA<sup>[77]</sup> conformers. Statistics relevant to the structure calculations are shown in Table 1. Sequence-specific resonance assignments were derived from presaturation DQF-COSY, 80 ms TOCSY and 250 ms ROESY spectra, largely by standard procedures. Data were analyzed with the aid of the XEASY program.<sup>[78]</sup> Distance restraints were obtained by integrating cross peaks in ROESY spectra and translating these into upper-distance limits by use of the

CALIBA module of DYANA. This program was also used to compute the structures by restrained molecular dynamics in torsion angle space by its standard simulated annealing protocol. Structures were optimized by molecular mechanics and superimposed for best fit, and rmsd values were obtained by use of the MOLMOL program.<sup>[75]</sup>

## Acknowledgements

The authors thank Prof. Raimund Dutzler (University of Zürich) for generous sharing of synchrotron beam-time, and Annelies Meier for technical assistance.

**Keywords:** beta-hairpins · p53–HDM2 · peptide nucleic acids · peptidomimetics · protein–protein interactions · secondary structure

- [1] D. Reichmann, O. Rahat, S. Albeck, R. Meged, O. Dym, G. Schreiber, *Proc. Natl. Acad. Sci. USA* **2005**, *102*, 57.
- [2] A. A. Bogan, K. S. Thorn, *J. Mol. Biol.* **1998**, *280*, 1.
- [3] T. Clackson, J. A. Wells, *Science* **1995**, *267*, 383.
- [4] T. Clackson, M. H. Ultsch, J. A. Wells, A. M. de Vos, *J. Mol. Biol.* **1998**, *277*, 1111.
- [5] L. Lo Conte, C. Chothia, J. Janin, *J. Mol. Biol.* **1999**, *285*, 2177.
- [6] P. L. Toogood, *J. Med. Chem.* **2002**, *45*, 1543.
- [7] J. A. Wells, *Proc. Natl. Acad. Sci. USA* **1996**, *93*, 1.
- [8] J. Späth, F. Stuart, L. Jiang, J. A. Robinson, *Helv. Chim. Acta* **1998**, *81*, 1726.
- [9] L. Jiang, K. Moehle, B. Dhanapal, D. Obrecht, J. A. Robinson, *Helv. Chim. Acta* **2000**, *83*, 3097.
- [10] M. Favre, K. Moehle, L. Jiang, B. Pfeiffer, J. A. Robinson, *J. Am. Chem. Soc.* **1999**, *121*, 2679.
- [11] A. Descours, K. Moehle, A. Renard, J. A. Robinson, *ChemBioChem* **2002**, *3*, 318.
- [12] J. A. Robinson, S. C. Shankaramma, P. Jetter, U. Kienzl, R. A. Schwendenner, J. W. Vrijbloed, D. Obrecht, *Bioorg. Med. Chem.* **2005**, *13*, 2055.
- [13] S. C. Shankaramma, Z. Athanassiou, O. Zerbe, K. Moehle, C. Mouton, F. Bernardini, J. W. Vrijbloed, D. Obrecht, J. A. Robinson, *ChemBioChem* **2002**, *3*, 1126.
- [14] S. C. Shankaramma, K. Moehle, S. James, J. W. Vrijbloed, D. Obrecht, J. A. Robinson, *Chem. Commun.* **2003**, 1842; Z. Athanassiou, R. L. A. Dias, K. Moehle, N. Dobson, G. Varani, J. A. Robinson, *J. Am. Chem. Soc.* **2004**, *126*, 6906.
- [15] R. Fasan, R. L. A. Dias, K. Moehle, O. Zerbe, J. W. Vrijbloed, D. Obrecht, J. A. Robinson, *Angew. Chem.* **2004**, *116*, 2161; *Angew. Chem. Int. Ed.* **2004**, *43*, 2109.
- [16] P. Chéne, *Nat. Rev. Cancer* **2003**, *3*, 102.
- [17] P. H. Kussie, S. Gorina, V. Marechal, B. Elenbaas, J. Moreau, A. J. Levine, N. P. Pavletich, *Science* **1996**, *274*, 948.
- [18] Note that mimetic **2** is identical to **78A** in the complete list of mimetics shown in Table 2.
- [19] O. Schon, A. Friedler, M. Bycroft, S. M. Freund, A. R. Fersht, *J. Mol. Biol.* **2002**, *323*, 491.
- [20] Z. Lai, K. R. Auger, C. M. Manubay, R. A. Copeland, *Arch. Biochem. Biophys.* **2000**, *381*, 278.
- [21] B. L. Sibanda, J. M. Thornton, *Methods Enzymol.* **1991**, *202*, 59.
- [22] B. Meyer, T. Peters, *Angew. Chem.* **2003**, *115*, 890; *Angew. Chem. Int. Ed.* **2003**, *42*, 864.
- [23] S. W. Homans, *Angew. Chem.* **2004**, *116*, 292; *Angew. Chem. Int. Ed.* **2004**, *43*, 290.
- [24] P. J. Hajduk, R. P. Meadows, S. W. Fesik, *Quart. Rev. Biophys.* **1999**, *32*, 211.
- [25] R. Stoll, C. Renner, P. Mühlhahn, S. Hansen, R. Schumacher, F. Hesse, B. Kaluza, R. A. Engh, W. Voelter, T. A. Holak, *J. Biomol. NMR* **2000**, *17*, 91.
- [26] O. Schon, A. Friedler, S. Freund, A. R. Fersht, *J. Mol. Biol.* **2004**, *336*, 197.
- [27] S. H. Gellman, *Curr. Opin. Chem. Biol.* **1998**, *2*, 717.
- [28] M. S. Searle, *J. Chem. Soc. Perkin Trans. 2* **2001**, 1011.
- [29] M. S. Searle, B. Ciani, *Curr. Opin. Struct. Biol.* **2004**, *14*, 458.
- [30] This mimetic **70** was erroneously described in the earlier communication<sup>[15]</sup> as a derivative with *N*-(2-methylpropyl)glycine at residue 4. The fourth residue is in fact *N*-(3-methylbutyl)glycine. The IC<sub>50</sub> (2.6 μM) and structural conclusions reported earlier are unchanged.
- [31] M. Rainaldi, V. Moretto, M. Crisma, E. Peggion, S. Mammi, C. Toniolo, G. Cavicchioni, *J. Pept. Sci.* **2002**, *8*, 241.
- [32] Y. Takeuchi, G. R. Marshall, *J. Am. Chem. Soc.* **1998**, *120*, 5363.
- [33] C. Garcia-Echeverria, P. Chéne, M. J. J. Blommers, P. Furet, *J. Med. Chem.* **2000**, *43*, 3205.
- [34] M. C. Lawrence, P. M. Colman, *J. Mol. Biol.* **1993**, *234*, 946.
- [35] L. T. Vassilev, B. T. Vu, B. Graves, D. Carvajal, F. Podlaski, Z. Filipovic, N. Kong, U. Kammlott, C. Lukacs, C. Klein, N. Fotouhi, E. A. Liu, *Science* **2004**, *303*, 844.
- [36] S. Uhrinova, D. Uhrin, H. Powers, K. Watt, D. Zheleva, P. Fischer, C. McInnes, P. N. Barlow, *J. Mol. Biol.* **2005**, *350*, 587.
- [37] S. K. Burley, G. A. Petsko, *Science* **1985**, *229*, 23.
- [38] C. A. Hunter, J. Singh, J. M. Thornton, *J. Mol. Biol.* **1991**, *218*, 837.
- [39] E. A. Meyer, R. K. Castellano, F. Diederich, *Angew. Chem.* **2003**, *115*, 1244; *Angew. Chem. Int. Ed.* **2003**, *42*, 1210.
- [40] M. A. McCoy, J. J. Gesell, M. M. Senior, D. F. Wyss, *Proc. Natl. Acad. Sci. USA* **2003**, *100*, 1645.
- [41] H. Adams, S. Cockcroft, C. Guardigli, C. A. Hunter, K. R. Lawson, J. Perkins, S. E. Spey, C. J. Urch, R. Ford, *ChemBioChem* **2004**, *5*, 657.
- [42] D. A. Dougherty, *Science* **1996**, *271*, 163.
- [43] S. K. Burley, G. A. Petsko, *FEBS Lett.* **1986**, *203*, 139.
- [44] M. T. Stubbs, S. Reyda, F. Dullweber, M. Müller, G. Klebe, D. Dorsch, W. W. K. R. Mederski, H. Wurziger, *ChemBioChem* **2002**, *3*, 246.
- [45] S. Maignan, J.-P. Guilloteau, Y. M. Choi-Sledeski, M. R. Becker, W. R. Ewing, H. W. Pauls, A. P. Spada, V. Mikol, *J. Med. Chem.* **2003**, *46*, 685.
- [46] N. Haginoya, S. Kobayashi, S. Komoriya, T. Yoshino, M. Suzuki, T. Shimada, K. Watanabe, Y. Hirokawa, T. Furugori, T. Nagahara, *J. Med. Chem.* **2004**, *47*, 5167.
- [47] M. Adler, M. J. Kochanny, B. Ye, G. Rumennik, D. R. Light, S. Biancalana, M. Whitlow, *Biochemistry* **2002**, *41*, 15514.
- [48] T. J. Tucker, S. F. Brady, W. C. Lumma, S. D. Lewis, S. J. Gardel, A. M. Naylor-Olsen, Y. Yan, J. T. Sisko, K. J. Stauffer, B. Y. Lucas, J. J. Lynch, J. J. Cook, M. T. Stranieri, M. A. Holahan, E. A. Lyle, E. P. Baskin, I.-W. Chen, K. B. Dancheck, J. A. Krueger, C. M. Cooper, J. P. Vacca, *J. Med. Chem.* **1998**, *41*, 3210.
- [49] G. Gerebtzoff, X. LiBlatter, H. Fischer, A. Frentzel, A. Seelig, *ChemBioChem* **2004**, *5*, 676.
- [50] S. J. Duncan, S. Gruschow, D. H. Williams, C. McNicholas, R. Purewal, M. Hajek, M. Gerlitz, S. Martin, S. K. Wrigley, M. Moore, *J. Am. Chem. Soc.* **2001**, *123*, 554.
- [51] S. J. Duncan, M. A. Cooper, D. H. Williams, *Chem. Commun.* **2003**, 316.
- [52] V. J. Huber, T. W. Arroll, C. Lum, B. A. Goodman, H. Nakanishi, *Tetrahedron Lett.* **2002**, *43*, 6729.
- [53] S. M. G. Knight, N. Umezawa, H.-S. Lee, S. H. Gellman, B. K. Kay, *Anal. Biochem.* **2002**, *300*, 230.
- [54] M. Kanovsky, A. Raffo, L. Drew, R. Rosal, T. Do, F. K. Friedman, P. Rubinstein, J. Visser, R. Robinson, P. W. Brandt-Rauf, J. Michl, R. L. Fine, M. R. Pincus, *Proc. Natl. Acad. Sci. USA* **2001**, *98*, 12438.
- [55] A. Böttger, V. Böttger, A. Sparks, W.-L. Liu, S. F. Howard, D. P. Lane, *Current Biol.* **1997**, *7*, 860.
- [56] V. Böttger, A. Böttger, S. F. Howard, S. M. Picksley, P. Chéne, C. Garcia-Echeverria, H.-K. Hochkeppel, D. P. Lane, *Oncogene* **1996**, *13*, 2141.
- [57] P. Chéne, J. Fuchs, J. Bohn, C. Garcia-Echeverria, P. Furet, D. Fabbro, *J. Mol. Biol.* **2000**, *299*, 245.
- [58] C. Garcia-Echeverria, P. Furet, P. Chéne, *Bioorg. Med. Chem. Lett.* **2001**, *11*, 2161.
- [59] R. Banerjee, G. Basu, P. Chéne, S. Roy, *J. Pept. Res.* **2002**, *60*, 88.
- [60] B. L. Grasberger, T. B. Lu, C. Schubert, D. J. Parks, T. E. Carver, H. K. Koblish, M. D. Cummings, L. V. LaFrance, K. L. Milkiewicz, R. R. Calvo, D. Maguire, J. Lattanze, C. F. Franks, S. Y. Zhao, K. Ramachandren, G. R. Bylebyl, M. Zhang, C. L. Manthey, E. C. Petrella, M. W. Pantoliano, I. C. Deckman, J. C. Spurlino, A. C. Maroney, B. E. Tomczuk, C. J. Molloy, R. F. Bone, *J. Med. Chem.* **2005**, *48*, 909.
- [61] J. A. Kritzer, J. D. Lear, M. E. Hodsdon, A. Schepartz, *J. Am. Chem. Soc.* **2004**, *126*, 9468.

- [62] J. A. Kritzer, M. E. Hodsdon, A. Schepartz, *J. Am. Chem. Soc.* **2005**, *127*, 4118.
- [63] M. M. Reddy, K. Bachhawat-Sikder, T. Kodadek, *Chem. Biol.* **2004**, *11*, 1127.
- [64] R. Stoll, C. Renner, S. Hansen, S. Palme, C. Klein, A. Belling, W. Zeslawski, M. Kamionka, T. Rehm, P. Muhlhahn, R. Schumacher, F. Hesse, B. Kaluza, W. Voelter, R. A. Engh, T. A. Holak, *Biochemistry* **2001**, *40*, 336.
- [65] I. R. Hardcastle, S. U. Ahmed, H. Atkins, A. H. Calvert, N. J. Curtin, G. Farnie, B. T. Golding, R. J. Griffin, S. Guyenne, C. Hutton, P. Kallbad, S. J. Kemp, M. S. Kitching, D. R. Newell, S. Norbedo, J. S. Northen, R. J. Reid, K. Saravanan, H. M. G. Willems, J. Lunec, *Bioorg. Med. Chem. Lett.* **2005**, *15*, 1515.
- [66] D. J. Parks, L. V. LaFrance, R. R. Calvo, K. L. Milkiewicz, V. Gupta, J. Lattanze, K. Ramachandren, T. E. Carver, E. C. Petrella, M. D. Cummings, D. Maguire, B. L. Grasberger, T. B. Lu, *Bioorg. Med. Chem. Lett.* **2005**, *15*, 765.
- [67] H. Yin, G. I. Lee, H. S. Park, G. A. Payne, J. M. Rodriguez, S. M. Sebti, A. D. Hamilton, *Angew. Chem.* **2005**, *117*, 2764; *Angew. Chem. Int. Ed.* **2005**, *44*, 2704.
- [68] L. H. Chen, H. Yin, B. Farooqi, S. Sebti, A. D. Hamilton, J. D. Chen, *Mol. Cancer Ther.* **2005**, *4*, 1019.
- [69] P. S. Galatin, D. J. Abraham, *J. Med. Chem.* **2004**, *47*, 4163.
- [70] W. Kabsch, *J. Appl. Crystallogr.* **1988**, *21*, 916.
- [71] J. Navaza, E. H. Panepucci, C. Martin, *Acta Crystallogr. Sect. D Biol. Crystallogr.* **1998**, *54*, 817.
- [72] G. N. Murshudov, A. A. Vagin, A. Lebedev, K. S. Wilson, E. J. Dodson, *Acta Crystallogr. Sect. D Biol. Crystallogr.* **1999**, *55*, 247.
- [73] G. M. Sheldrick, T. R. Schneider, *Methods Enzymol.* **1997**, *277*, 319.
- [74] A. Nicholls, K. Sharp, B. Honig, *Proteins* **1991**, *11*, 281.
- [75] R. Koradi, M. Billeter, K. Wüthrich, *J. Mol. Graphics* **1996**, *14*, 51.
- [76] R. M. Esnouf, *J. Mol. Graphics Modell.* **1997**, *15*, 132.
- [77] P. Güntert, C. Mumenthaler, K. Wüthrich, *J. Mol. Biol.* **1997**, *273*, 283.
- [78] C. Bartels, T. Xia, M. Billeter, P. Güntert, K. Wüthrich, *J. Biomol. NMR* **1995**, *6*, 1.

---

Received: November 2, 2005